



IARIW 2025

# IARIW 2025

Thursday, October 2 & Friday, October 3

## **One-Fifth of the World's Population at High Risk from Climate-Related Hazards**

Ben Brunckhorst

Stephane Hallegatte

Ruth Hill

Minh Nguyen

Esther Naikal






Nisan Gorgulu

(World Bank)

Paper prepared for the IARIW–World Bank–UEB/VNU Conference on “Improving Well-being Measurement in Data-challenged Environments in Developing Countries for Better Evidence-based Policies” October 2-3, 2025

Session 1 Plenary: Improving Welfare Measurement  
Time Slot: Thursday, October 2, 10:15-12:15 PM

## **One-fifth of the world's population at high risk from climate-related hazards**

Ruth Hill  Nisan Gorgulu  Ben Brunckhorst  Minh Cong Nguyen   
Stephane Hallegatte  Esther Naikal

### **Abstract**

Climate change is increasing the frequency and intensity of extreme weather events. When these events occur, they threaten lives and livelihoods. Here we estimate the global population at high risk from climate-related hazards by examining household level vulnerability and local exposure to four types of events: agricultural droughts in rural areas, floods, heatwaves, and cyclones. Under current climate conditions, 4.5 billion people are expected to experience these hazards at intensities exceeding critical thresholds within their lifetime. One third of this population is considered highly vulnerable, based on seven dimensions that influence potential welfare impacts: income, education, access to finance, social protection, drinking water, electricity, and access to services and markets. Overall, we estimate that 1 in 5 people globally are at high risk from these hazards meaning that they are likely to experience them and would struggle to recover from their impacts. While the proportion of the population at high risk has nearly halved since 2010 due to decreased vulnerability, the number of people exposed has increased, and progress has been uneven across regions. This study offers a new global population headcount indicator based on household survey and high-resolution spatial data that will be used to track climate risks across countries and over time.

## Main

At any time, some households are experiencing welfare gains and moving out of poverty, whilst others are experiencing setbacks and falling into poverty<sup>1</sup>. Poverty reduction, and development more broadly, requires both advancing welfare and protecting households from setbacks. One major cause of setbacks are climate-related hazards, which are increasing in frequency and intensity with climate change<sup>2,3</sup>. Not only do they increase poverty when they occur, they cast a long shadow on welfare, as they can result in losses to assets, health and natural capital that limit welfare gains for many years to come. Vulnerable households are sometimes forced to adopt costly coping strategies, such as reducing spending on health and education, or selling productive assets, which can affect people's – and especially children's – prospects for decades<sup>4</sup>.

Sustainable development and poverty reduction require reducing the number of people who are at risk from extreme weather events. Tracking global progress on this goal demands an indicator that can be measured consistently across countries and over time. Existing approaches to measure climate risk or vulnerability typically model aggregate economic losses or combine country level metrics in an index<sup>5,6,7,8,9,10</sup>. Instead, we use a people-centric and threshold-based approach: we count people at high risk and produce a population headcount indicator similar to what is used to monitor global poverty<sup>11</sup>. In spite of the simplification it requires, the extreme poverty headcount indicator (the number of people living on less than \$2.15 per day) has proven immensely valuable to global development efforts because it is transparent and easily understandable to the public and makes it possible to track progress (or the absence thereof). Our approach provides practical innovations over existing metrics as it explicitly weights every person equally, allows for simple decompositions, and provides a flexible methodology that can be adapted to local contexts by selecting different thresholds (analogous to the different poverty lines). This new risk indicator has been adopted by the Multilateral Development Banks Common Approach to Measuring Climate Results and is being used by the World Bank Group as one measure of progress towards ending poverty on a livable planet<sup>i</sup>. It will be regularly updated and publicly available.

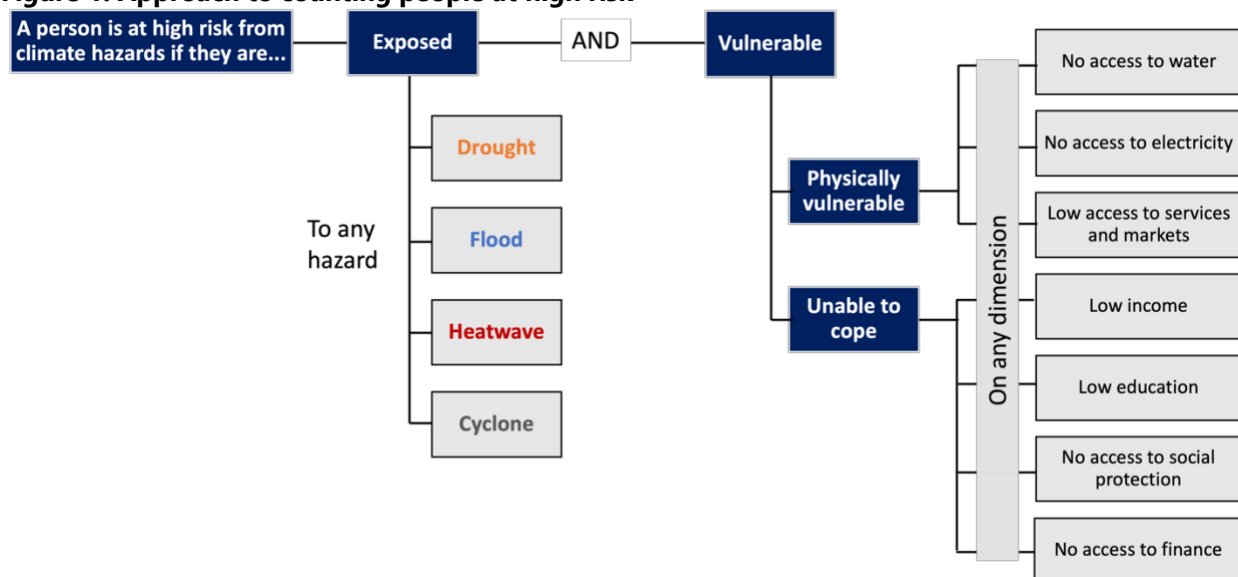
In this study, we present the indicator methodology and estimate the number of people at high risk from climate-related hazards globally around 2021, and the trend since 2010. We follow the traditional framework in which risk is the combination of hazard, exposure, and vulnerability<sup>12</sup>. Hazard is the potential occurrence of an extreme event; exposure is the presence of people in places or settings that could be adversely affected; and vulnerability is the propensity or predisposition of these people to be experience losses when they are affected.

---

<sup>i</sup> <https://scorecard.worldbank.org>

Everybody faces some level of risk from extreme weather events, and everyone is vulnerable to some extent. To provide a meaningful metric, we consider thresholds that focus on exposure to *severe* events and *high* levels of vulnerability. We identify people at high risk from climate-related hazards as those who are both exposed and likely to suffer severe consequences (i.e., who are highly vulnerable). Figure 1 summarizes our approach. The exposed population is estimated using spatial datasets derived from remote sensing and hazard modeling, whereas vulnerability is largely measured from household surveys (see Methods). The result is an estimate of the number of people likely to experience substantial welfare losses due to climate hazards in their lifetime.

**Figure 1: Approach to counting people at high risk**



### Global exposure to extreme weather events

We examine exposure to four types of climate-related hazards: agricultural droughts, floods, heatwaves, and tropical cyclones. The exposed population is defined as those living in areas where these events exceed a critical intensity threshold with at least some frequency (Table 1). We consider whether events exceed intensity thresholds under current climate conditions with an annual frequency of at least 1% (a return period of 100 years). This translates to at least 52% probability over the average life expectancy of 72 years such that people are more likely than not to experience these events in their lifetime. Each type of hazard has distinct impacts, affecting lives, productivity, or assets in different ways. The multidimensional nature of impacts means no single metric would make exposure thresholds equally severe across hazards, it depends on how one weights mortality and morbidity impacts, food security, economic losses, and many other factors. Here, we use critical thresholds for each type of hazard based on existing vulnerability studies or risk assessments.

Locations exposed to severe agricultural drought are defined using the “severe drought” definition of the FAO’s Agricultural Stress Index (ASI) in rural areas<sup>13,14</sup>. We define exposed locations as those where more than 30% of the land area experienced severe drought (ASI > 30) for any season over 39 years with observations<sup>15</sup>. We consider pluvial, fluvial and coastal flooding using modelled probabilistic inundation maps from Fathom and Deltares<sup>16,17</sup>. Locations are considered exposed to severe flooding if the maximum inundation depth exceeds 0.5 m from any type of flooding with an annual frequency of at least 1%. Floods above this level are associated with disruptions to livelihoods and economic activities and characterized as “high risk” in the literature<sup>18</sup>. Estimates of the share of residential assets lost from a 0.5 m fluvial flood range between 22-49% across regions<sup>19</sup>. Exposure to severe tropical storms is based on the modelled STORM wind speed data for different return periods<sup>20,21</sup>. Locations where wind speeds reach at least Category 2 on the Saffir-Simpson scale with an annual frequency of at least 1% are defined as exposed. Cyclones of this intensity are associated with damages to buildings and infrastructure<sup>22,23</sup>. For heatwaves, we defined exposed locations as those where the 5-day mean of daily maximum Wet-Bulb Globe Temperature (WBGT) exceeds 33°C with an annual frequency of at least 1%. This corresponds with the reference upper limit for healthy, acclimatized humans at rest to keep a normal core temperature<sup>24</sup>. At this temperature, heat-related mortality and hospital visits increase, and physical work capacity is reduced to around 50%<sup>25,26,27</sup>. WBGT is approximated using the Environmental Stress Index (ESI), derived from hourly ERA5 reanalysis<sup>28,29</sup>.

**Table 1: Hazard thresholds defining an exposed location**

<b>Hazard</b>	<b>Annual frequency</b>	<b>Intensity</b>
Agricultural drought	≥ 1/39 years in historical record	>30% cropland or pasture affected and rural
Flood	≥ 1%	> 0.5 m inundation depth
Heatwave	≥ 1%	>33°C 5-day mean of daily maximum WBGT
Tropical cyclone	≥ 1%	≥ Category 2 wind speed

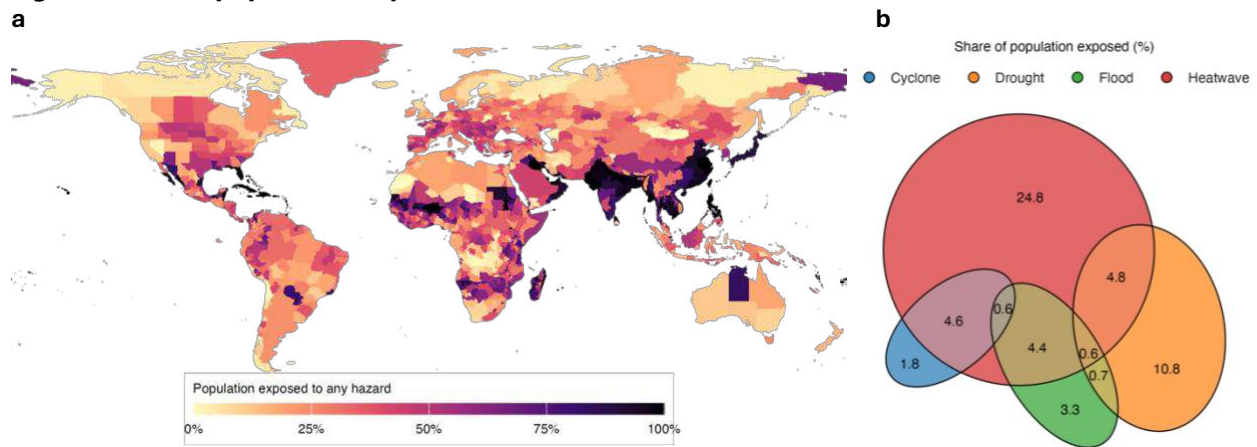
We estimate that 4.5 billion people, or 57% of the global population, are exposed to at least one hazard that exceeds the thresholds defined in this study. Figure 2a maps the share of population exposed to any hazard. The share exposed is higher in South Asia (87%) and East Asia and the Pacific (69%), but local hotspots exist within every region (Extended Data Table 1). If we restrict exposed locations to those where the same intensity thresholds are exceeded with an annual frequency of at least 5%, instead of at least 1%, the global population exposed to any hazard is reduced to 47% (Extended Data Table 2). To explore the sensitivity of results to these thresholds, estimates of the population considered exposed with a wide range of intensity and frequency thresholds are included in the Supplementary Information.

Our method assigns every population grid cell (approximately 90 x 90 m) to one of 16 exposure categories representing all possible combinations of hazards. This prevents double counting while allowing analysis of exposure to multiple hazards, as shown in Figure 2b. Heatwaves are the hazard with highest share of the population exposed (40%) and

dominate in regions closer to the equator (Extended Data Figure 1). Around three quarters of those exposed to cyclones (8% of the total population) and more than half of those exposed to floods (10%) are also exposed to heatwaves, influenced by tropical weather patterns, topography and urbanization in these locations. A substantial share of the population is exposed to severe droughts (17%), considering this only counts people in rural areas, of which more than a third are exposed to another type of hazard. Overall, 16% of the population are exposed to more than one above-threshold hazard but only 1.6% are exposed to more than two. Figure 2b does not visualize very small intersections such as the population exposed to all four hazards exceeding thresholds (0.04%), and there are people exposed to every possible hazard combination.

We also classify the population by degree of urbanization, in order to subsequently merge exposure with survey-based vulnerability indicators specific to the rural and urban population. Almost three quarters of the rural population, defined by the degree of urbanization methodology<sup>30</sup>, are exposed to severe drought. However, a relatively larger share of the urban population is exposed to cyclones, floods and heatwaves (Extended Data Table 3). Exposure to flooding is highest in peri-urban and suburban areas on the outskirts of cities (12% of the population), where formal land-use planning may be less common. Results highlight varying rates of population exposure across urbanization levels and the need for tailored risk management strategies.

**Figure 2: Global population exposed to four hazards**



**a.** Map showing the share of population exposed to any of the four climate-related hazards exceeding intensity thresholds for a given return period event (Table 1). Estimates are aggregated to the lowest level representative spatial units in household surveys used to assess vulnerability, or to country level if household surveys are not available. **b.** Euler diagram showing the share of the global population exposed to each combination of hazards. Note intersections accounting for less than 0.5% of the population are not shown, however exposure rates are greater than zero for all possible combinations (e.g., all four hazards).

## **Vulnerability to extreme weather events**

To identify the population that is highly vulnerable, we use seven indicators that proxy different dimensions of vulnerability (Figure 1). These are informed by a large literature studying the type of households with a high probability of experiencing severe losses when exposed to extreme weather events. They capture both a household's physical propensity to experience loss of income, assets or health and their inability to cope with and recover from losses. Each dimension is defined with a threshold, selected based on existing literature and available data. Because we aim at identifying people "highly" vulnerable at the global level, these thresholds are low. Studies that focus on specific populations – such as very poor or very rich countries – could apply the same approach using different thresholds more appropriate to their context.

A household is considered highly vulnerable if they are vulnerable on any dimension. This approach gives an equal importance to each dimension. In reality, certain dimensions may be more critical depending on the context or type of hazard, and the interaction between dimensions may be important. Our approach does not currently incorporate this complexity; however, we demonstrate the potential for such extensions by mapping the complete joint distribution of hazard exposure and vulnerability dimensions (Extended Data Figure 4).

The specific indicators were selected because they have well-recognized global definitions and are widely available in survey data. They are mostly derived from household surveys that are representative of the population at subnational rural-urban level, allowing global scale analysis of the population at risk with unprecedented granularity. Most indicators are derived from harmonized household survey microdata available from the World Bank's Global Monitoring Database (GMD), while others are fused into the GMD household surveys using the Findex microdata for access to finance and ASPIRE data for social protection (see Methods and the replication package for details)<sup>31,32</sup>. The GMD is the World Bank's repository of multitopic income and expenditure household surveys used to monitor global poverty<sup>33</sup>. The household survey data are typically collected by national statistical offices in each country, and then compiled, processed, and harmonized by the World Bank such that levels and trends in key sociodemographic attributes can be reasonably compared across and within countries over time<sup>34</sup>. Since we use the exact same underlying microdata, our indicators are consistent with official monetary and multidimensional poverty statistics published by the World Bank. For 2021 estimates, we use data from 160 nationally representative household surveys with a combined sample size of over 11 million individuals (surveys are listed in the Supplementary Information).

Physical propensity to experience severe loss is proxied using three indicators. Households are considered highly vulnerable if they lack access to improved drinking water. Improved sources of water can protect people from contamination when storms and floods occur or

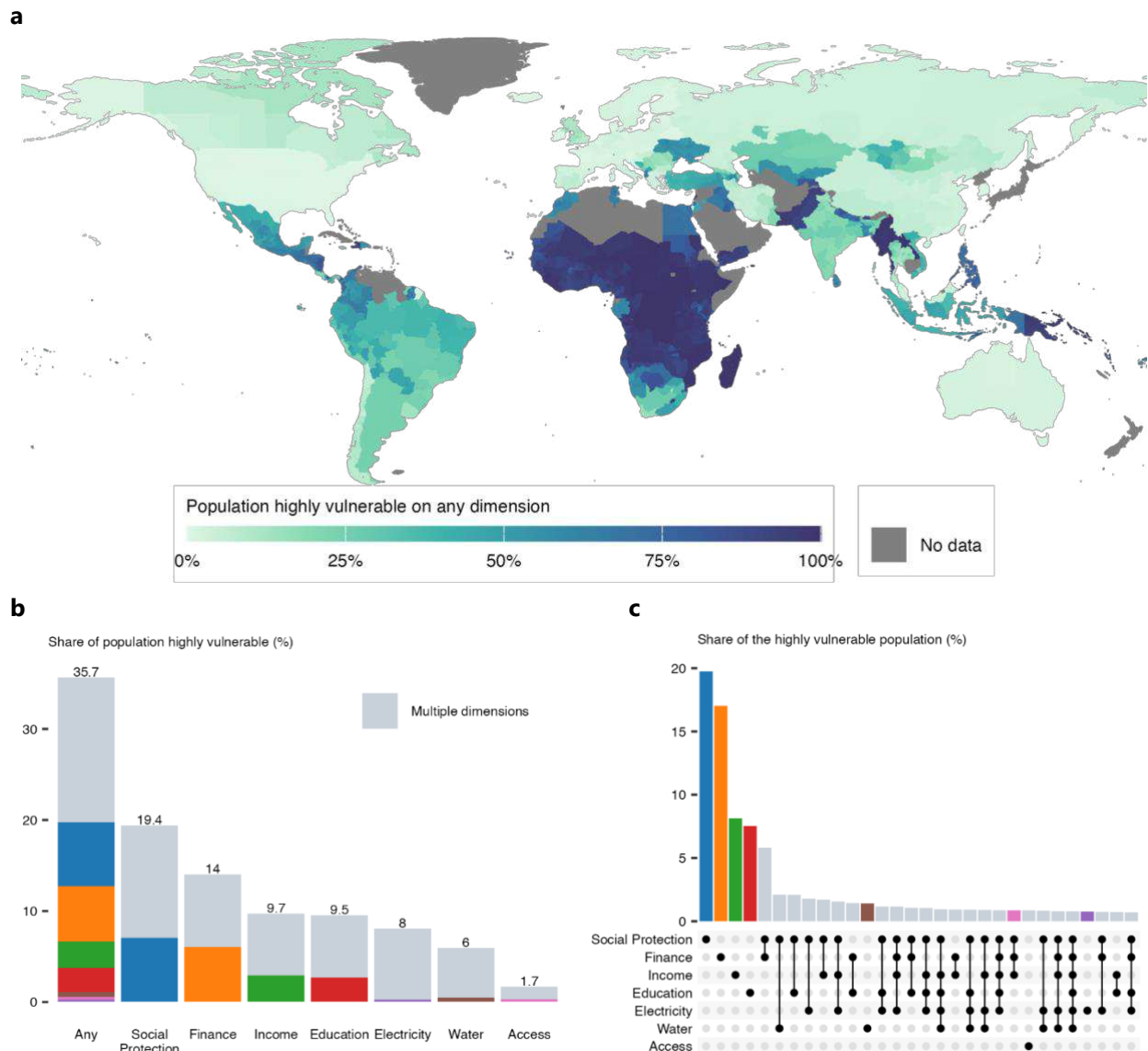
lessen the impacts of droughts and heatwaves<sup>35</sup>. Households are also considered highly vulnerable if they lack access to electricity. During heatwaves, households with electricity are much more likely to have fans or other devices that can alleviate impacts. Lastly, access to services and markets enhances resilience by providing access to healthcare and other support, and ensuring households can access alternate employment opportunities and markets for goods (including food when local production fails)<sup>36</sup>. Households are considered highly vulnerable if they are rural and located more than 2 km from an all-season road, consistent with the Rural Access Index (SDG 9.1.1).

Inability to cope with losses is proxied using four indicators. First, households are considered highly vulnerable if they live below the international poverty line of \$2.15 (2017 PPP) per person per day (Income dimension). Should a hazard occur, they would be unable to meet basic needs. Second, households are considered highly vulnerable if no adult member has completed primary education (Education dimension). Educational attainment captures both the ability to understand and respond to information such as early warnings, as well as the ability to switch livelihoods when faced with climate-related hazards<sup>37,38,39,40</sup>. Third, households are considered highly vulnerable if they do not have access to a bank or mobile money account (Finance dimension). Borrowing money or accessing transfers from family members is a widespread and effective coping strategy in the aftermath of a disaster<sup>41,42,43</sup>. Access to a bank or mobile money account increases the geographical reach of these transfers so that they can be used to manage climate shocks. Fourth, there is considerable evidence that public cash transfers and other social protection systems help households manage shocks<sup>44,45,46,47,48,49,50</sup>. Ideally, to measure this dimension we would use data on whether a household can be covered by social protection should a crisis occur. The number of beneficiaries at one point in time may be a poor proxy for this potential coverage, especially where adaptive social protection systems may scale up in times of crisis. So instead of using transfers only, we assume that only households neither receiving social protection transfers nor contributing to social insurance are highly vulnerable (Social Protection dimension)<sup>51,52,53</sup>.

The share of the global population highly vulnerable on each dimension in 2021 ranges from 2% (access to services and markets) to 19% (access to social protection), based on surveys from 160 countries representing 94% of the global population (Extended Data Table 4). 14% of people lack access to finance and 6-10% are considered highly vulnerable on the remaining dimensions. The share of population highly vulnerable on any dimension in 2021 is 36% in our sample. Figure 3a maps the stark differences in vulnerability across the globe. Sub-Saharan Africa has 90% of its population highly vulnerable on at least one dimension, whereas less than 3% are highly vulnerable in high income countries. The dimension on which the largest share of the population is vulnerable varies substantially across countries (Extended Data Figure 2).

While one could expect income to be a good proxy for other dimensions of vulnerability, the correlation across dimensions is not particularly high (Extended Data Figure 3). This is underscored by the fact that although two-fifths of those highly vulnerable are vulnerable on multiple dimensions (16% of the global population), three fifths are vulnerable on one dimension only (Figure 3b). This emphasizes the different nature of vulnerability across households, and the diversity of resilience-enhancing policies required in different places, even within countries. Lack of access to social protection and lack of financial inclusion are most common among those vulnerable on a single dimension (Figure 3c).

**Figure 3: Share of population highly vulnerable, on any or several dimensions**



**a.** Map showing the share of population vulnerable on any dimension for 2021. Estimates are aggregated to the lowest level representative spatial units in household surveys. **b.** Chart showing the share of the total population vulnerable on any dimension and on each dimension. The columns are stacked by the proportion vulnerable on a single dimension and on multiple dimensions. **c.** Upset plot showing the relative share of the vulnerable population on each combination of dimensions. The 30 most common combinations are shown.

## The global population at high-risk

We estimate the population at risk from climate-related hazards by merging the population exposure estimates derived from high resolution spatial data with information on household vulnerability from surveys. People at high risk are defined as those exposed to any hazard and vulnerable on any dimension, based on specific thresholds (Figure 1). We find that almost 1 in 5 people (19%) are at high risk from climate-related hazards based on data from 160 countries for 2021 (Extended Data Table 5).

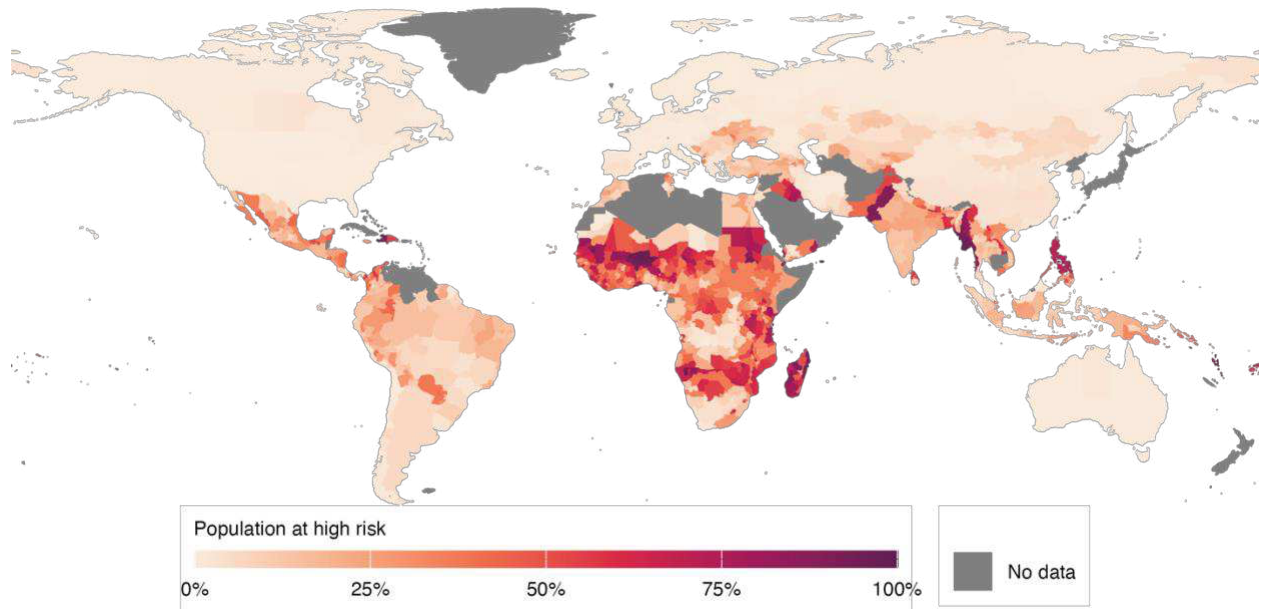
Figure 4a maps the share of population at high risk in 2021, highlighting spatial inequalities arising from the intersection of exposure and vulnerability. Nearly everyone who is exposed in Sub-Saharan Africa is considered highly vulnerable and therefore at high risk. Sub-Saharan Africa had the highest vulnerability rates for 2021 (8-71%) on each dimension except access to finance (30%), which is also high in the Middle East and North Africa (39%). In contrast, Asia has higher rates of population exposure on average, but lower vulnerability. Population exposure is similar in North America and Latin America and the Caribbean at the region level, but there is a considerable difference in the share at high risk because very few are counted as highly vulnerable in North America when using our thresholds. There are 37 economies, many of them small islands, where the entire population is exposed to cyclones or heatwaves exceeding intensity thresholds, but among these the population at high-risk ranges from less than 1% (Taiwan) to over 90% (Haiti) due to differences in vulnerability. The map also highlights significant variation within countries with subnational data.

We find 8% of the population are exposed and vulnerable on more than one dimension. People in sub-Saharan Africa and those exposed to drought are particularly likely to be highly vulnerable on multiple dimensions. Of those exposed to drought, three fifths are highly vulnerable on multiple dimensions, while this is closer to one third for people exposed to other hazards (Figure 4b). These exposed populations facing multiple deprivations are more likely to require systematic and targeted support to become more resilient. We further decompose results to quantify the population exposed to each combination of hazards and facing each combination of vulnerabilities (Extended Data Figure 4). This detail is useful for informing context sensitive and multifaceted climate change adaptation strategies.

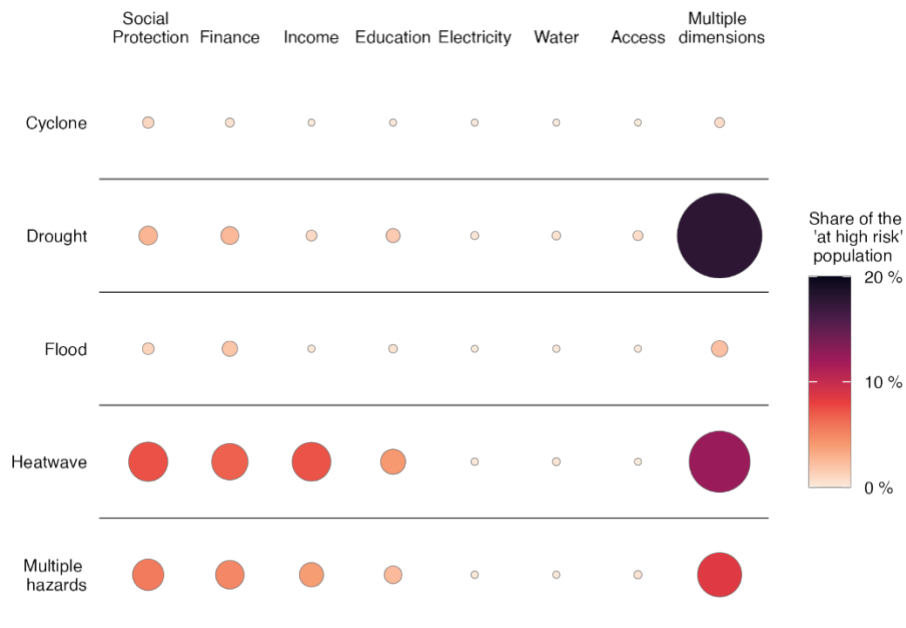
The approach can be adapted to use locally appropriate thresholds and more granular data needed for implementing local adaptation plans. Applying the method to high-income countries in North America and Europe could use higher thresholds, analogous to the use of higher poverty lines in richer countries than what is used to monitor global poverty. In this study our focus is on those most exposed and highly vulnerable at the global level. The Supplementary Information offers details on the sensitivity to the choice of thresholds.

**Figure 4: Share of population at high risk**

**a**



**b**



**a.** Map showing the share of population at high risk from climate-related hazards. Estimates are aggregated to the lowest level representative spatial units in household surveys used to assess vulnerability. **b.** Chart showing the relative share of the population at high risk by the hazard(s) they are exposed to and dimension(s) they are vulnerable on. The population exposed to more than one hazard and vulnerable on more than one dimension are each aggregated to one joint category (“Multiple...”). The size and color of circles represent the relative share of the population.

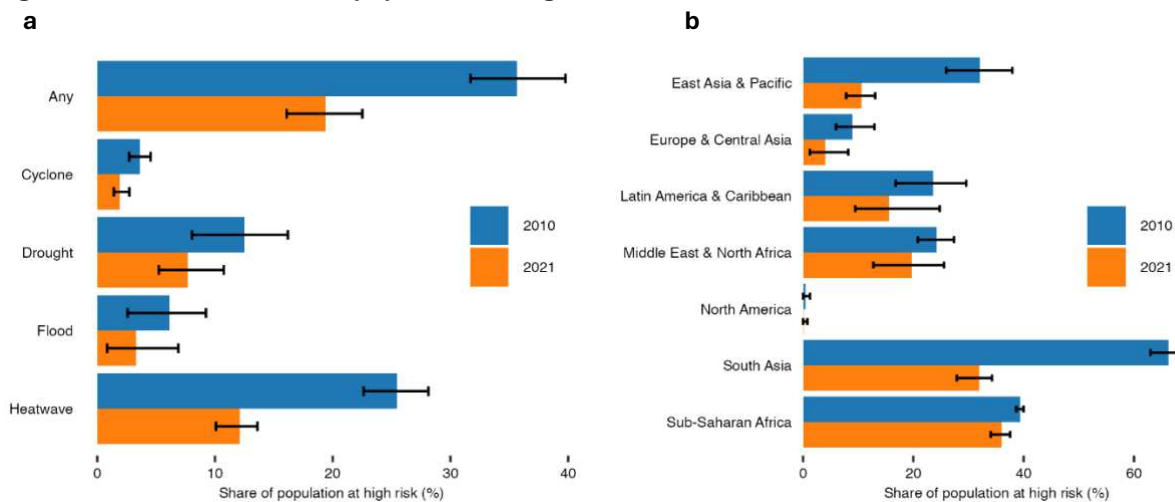
## Historical trends

We estimate recent trends in those at high-risk by examining how the number of people exposed and vulnerable have changed between 2010 and 2021. Constraints on data availability in 2010 require us to make additional simplifications. While it is likely that the frequency and intensity of weather extremes has shifted to some extent over this period, it is considerably shorter than the 20-to-30-year timescale typically required to robustly measure changes in the climate. We therefore assume constant climate conditions between 2010 and 2021. We also assume two dimensions of vulnerability (access to social protection and access to services and markets) are constant due to lack of available time trend data.

With these caveats, the share of the global population at high risk from climate hazards has decreased substantially from over 1 in 3 people in 2010 (2.5 billion) to 1 in 5 in 2021 (1.5 billion) (Figure 5a). The trend can be attributed almost entirely to a decrease in severe levels of vulnerability among households in exposed locations. The share of people living in exposed locations did not change significantly at the global level as a result of net-migration and differences in population growth between exposed and unexposed places, however the absolute number of people exposed increased by 461 million. Trends in exposure for specific locations and hazards vary, for instance our results are consistent with evidence that cities are growing faster in flood zones than in safe areas<sup>54</sup>.

Globally, the largest decrease in vulnerability was on the access to finance dimension. The share of the exposed population without a bank or mobile money account decreased from 21% in 2010 to 8% in 2021, highlighting rapid improvements in financial inclusion over the last decade (Extended Data Table 5). The share of exposed people highly vulnerable on income, education and access to infrastructure dimensions have each decreased by around half. The decrease in the population at high-risk over the last decade has been driven by development in some highly populated and exposed regions, with seemingly limited progress occurring in others. South Asia and East Asia & Pacific regions saw the largest decreases in their populations at high-risk, dropping from 66 to 32 percent and 32 to 11 percent respectively, due to significant improvements across most vulnerability dimensions (Figure 5b).

**Figure 5: Trend in the share of population at high risk from climate-related hazards, 2010 to 2021**



**a.** Chart showing the global share of population at high risk over time from any climate-related hazard with return period of 100 years, and any dimensions of vulnerability. Intervals show the full extent of uncertainty (100% confidence interval) from assuming zero correlation between exposure and vulnerability within survey statistical regions. **b.** Chart showing the share of population at high risk over time and by geographical regions. 100% confidence intervals for one source of uncertainty are shown (as in a.).

## Discussion

Assessing climate risk is complex and data intensive, requiring information on hazards, the people and assets exposed, and the extent that those exposed would be adversely affected. A comprehensive risk assessment would ideally integrate probabilistic models to estimate welfare losses, beyond just monetary impacts. This exists for some losses from some types of events.<sup>5</sup> However, the modelling involved is highly uncertain and remains challenging to communicate to a broad audience. The population headcount indicator we develop instead follows a simple approach, counting the number of people at high risk globally by applying exposure thresholds and proxies for vulnerability. While it does not replace more sophisticated models, it serves as a complementary tool, offering a practical alternative for assessing climate risks, especially in data-limited contexts.

By providing a more granular, people-focused metric, our indicator also complements existing global risk and vulnerability indices such as the Global Climate Risk Index, the UN Multidimensional Vulnerability Index, INFORM, and ND GAIN. Compared to these indices, our approach allows for more spatially granular insights and integrates often overlooked dimensions of vulnerability by merging high resolution spatial and household survey data. As opposed to composite indices, our headcount indicator can be decomposed by geography (at subnational level) and population group (e.g., urban/rural, or per income quintile), as well as the hazards people are exposed to and the (multiple) dimensions on which they are highly vulnerable. This provides a more nuanced understanding of

vulnerability in the population exposed to climate shocks within countries. Moreover, our method can be used to develop local versions of the indicator that use appropriate contextual thresholds for both exposure and vulnerability, in the same way that country-specific poverty lines differ from international poverty lines.

Nonetheless, limitations related to data availability and aggregation remain. The threshold approach allows to develop a population headcount indicator, but one limitation is that beyond these thresholds we do not distinguish between people exposed more frequently or to more intense events. Our approach only counts people exposed to severe above-threshold hazard events. It does not account for low-intensity, high-frequency events that, while individually less severe, may cause significant cumulative damage over time. The Supplementary Information includes estimates using a wide range of intensity and frequency thresholds to define exposed locations. For the global indicator, we focus solely on four types of climate-related hazards and exclude environmental factors like air pollution. This means the numbers presented do not reflect all climate-related risks to welfare. To identify people at high risk today, we consider the probability of hazards in the current climate. We do not project exposure to hazards in a future climate scenario, but this can be done using our methodology and will be part of future work.

Our analysis focuses on direct exposure to climate-related events, considering who is in the path of an event, rather than who may experience indirect effects such as disruption to markets, price fluctuations, or the consequences of damage to infrastructure. Moreover, the calculation method does not consider the cascading effects that often follow disasters, like propagation of impacts through supply chains, migrations from affected areas, or the outbreak of diseases that can sometimes occur in the aftermath of such events. While this means that our results underestimate the total number of people at risk, they remain a reliable proxy, as indirect effects stem from direct population exposure.

In measuring vulnerability, our approach focuses on extreme levels of vulnerability, acknowledging that vulnerability can be defined differently in different contexts and in countries at different income levels, and that even people who are not considered at high risk in our methodology can be severely affected by an extreme event. Our method assigns equal importance to each vulnerability dimension, such as access to infrastructure or financial inclusion. However, the importance of each dimension can vary depending on the context and specific hazard. There are also important dimensions of vulnerability for which it was not possible to find an indicator with significant global coverage to use in this analysis. Access to health services, demographic factors such as age and measures of social or political exclusion are key dimensions of vulnerability that were not included for this reason. While the former could be addressed through data investments, the latter is more challenging to measure consistently across contexts.

Finally, data limitations remain a challenge even for the dimensions of vulnerability included. We identify three main challenges and areas for future work. First, our approach requires data on multiple dimensions for the same household. Since data on all dimensions is not available from the same household survey, indicators from different sources must be fused together. Work to further develop data fusion methods is warranted to better capture the overlap between vulnerability dimensions. Ongoing efforts to improve and standardize household surveys are also critical so that indicators measuring different dimensions of vulnerability are collected in the same survey.

Second, vulnerability data are generally available at the subnational level, a much larger geographical area than the grid-level exposure estimates. When overlaying the two, we assume that the share of highly vulnerable households is the same in exposed locations as in those not exposed to hazards. This assumption is more plausible for smaller areas with similar households but may not hold for larger regions, especially in heterogeneous urban areas. To assess the size of potential bias from making this assumption, we estimate upper and lower bounds by instead assuming maximum and minimum overlap between exposed and vulnerable populations within subnational areas (100% confidence intervals shown in Figure 5). The difference between estimates at these bounds was less than three percentage points in subnational areas accounting for most of the global population. However, the potential bias is larger when surveys represent populations dispersed over large regions, and more spatially disaggregated data is needed to reduce this uncertainty (see Methods and Supplementary Information).

Third, in many cases key data – such as coverage by social protection systems or intra-household disparities – are either incomplete or unavailable for all countries. For instance, data on access to basic water services is not consistently included in surveys, and information on social protection beneficiaries is not available for all countries and often relies on modeled estimates rather than direct reporting. In many cases data on the different dimensions of vulnerability are not up to date, with information from different years often combined, which can lead to inconsistencies. Continued investments are needed in household survey data to ensure this measure becomes more accurate over time.

Unfortunately, there is no quick fix to the data gaps at the global level, including for the selection of more or different vulnerability thresholds, or the quantification of the relative importance of different vulnerability dimensions. Improving the data for resilience measurement is at least a 5- to 10-year effort to improve household data collection methods, strengthen the capacity of national statistics office, and implement such enhanced data collection in all countries. Initial efforts are underway, but meeting short term needs to inform policy decisions requires to cope with the current data availability constraints.

In spite of these limits, the approach proposed here can provide an important tool to help prioritize actions across countries, hazards, and sectors, and to improve accountability through consistent and transparent monitoring of the world progress in building resilience. There is a strong precedent showing the value of such population headcount indicators in global development. The extreme poverty indicator has been a game changer for consistently tracking poverty because it is easily understandable to both the public and policymakers and rigorously estimated from household survey data using transparent methods. We follow the same principles to count the number of people at high risk from climate related hazards. The resulting indicator complements the suite of existing global climate risk indices by providing an interpretable and people-centric metric that can be used to monitor progress across countries and over time.

## Methods

We follow three steps to identify those at high risk from climate-related hazards. First, the number of people living in locations exposed to extreme weather events is calculated by overlaying hazard maps and gridded population data. Second, the share of people highly vulnerable across several dimensions is calculated by fusing indicators derived from household surveys and other sources. These estimates are representative of the population in a specific geographic region (typically subnational) and can therefore be linked to the exposure data. The final step calculates the number of people who are at high risk by combining exposure and vulnerability estimates from the previous steps for the same location and population group. Extended Data Figure 5 provides a visual summary of the method. The following sections describe the methods and data used in each step. A reproducibility package containing code used for analysis and data availability statements is available.

### Step 1 - Determining who is exposed

The exposed population is estimated by combining global gridded population, degree of urbanization and hazard maps. The hazard maps (available from various data sources below) depict the intensity of a given return period (frequency) event. To define exposed locations, we combine intensity and frequency: exposed locations are defined as those where each hazard exceeds a given intensity threshold with a frequency that exceeds a given threshold (Table 1 and Figure S1 in Supplementary Information). The degree of urbanization data is used to classify the population so that we can later merge vulnerability information specific to the rural or urban population. The hazard and degree of urbanization spatial data is first resampled so that grid cells align with the 3 arcsecond (approximately 90 m) resolution population data. We classify every population grid cell covering the globe (approximately 90 billion) by exposure to any combination of the four hazards, and by eight degree of urbanization categories. As a result, the global population is assigned to one of 128

possible exposure-urbanization categories at a very fine spatial scale (see Extended Data Figure 5). The population in each exposure-urbanization category is aggregated from grid level using boundaries corresponding with the representative statistical regions in the household surveys used to assess vulnerability. When statistical regions partially cover a grid cell, the population assigned to that region is weighted by the cell coverage fraction.

The following sections describe the spatial population, hazard and boundary data used. Most datasets are publicly available and full data availability statements are included in the reproducibility package.

### **Population data**

To map the population, we use GHS-POP data from the Global Human Settlement Layer (GHSL)<sup>55</sup>. The dataset depicts the residential population at a resolution of 3 arcseconds, derived from the Gridded Population of the World version 4.11 (GPWv4.11), and disaggregated to grid cells informed by the distribution, classification, and volume of built-up areas also mapped by the GHSL<sup>56</sup>. The populations of GHSL are well suited for merging with survey data since they are closer to statistical values than alternatives such as WorldPop because the spatialization method maintains the population in the administrative or census region<sup>57</sup>. We use the 2010 and 2020 global data files.

To classify the population so that we can merge vulnerability information specific to the rural or urban population, we use GHS-SMOD gridded data from GHSL which applies the Degree of Urbanisation methodology recommended by the UN Statistical Commission<sup>58</sup>. Settlements are classified according to population cluster sizes, population densities and built-up area densities, as defined by the stage I of the Degree of Urbanisation, at a spatial resolution of 1km globally<sup>30</sup>. Although the vulnerability data is only available for rural and urban subgroups, we classify the exposed population by seven degree of urbanization subcategories depicted by GHS-SMOD to improve our ability to match the definition used by surveys which varies across countries (described in Step 3).

Population estimates derived from GPWv4.11 are based on outdated census in some countries. For consistency with the population used for global poverty monitoring and other statistics, we use country population data from the World Bank's World Development Indicators (WDI) to rescale estimates extracted from gridded data<sup>59</sup>.

### **Hazard data**

For agricultural drought, we use Historic Agricultural Drought Frequency maps from the FAO. The data depicts the annual frequency of severe drought in up to two growing seasons where more than 30% of cropland or grass-land is affected, according to the Agricultural Stress Index (ASI), with a spatial resolution of 1 km<sup>15</sup>. The ASI is based on remote sensing vegetation (NDVI) and land surface temperature (BT4) data, combined with information on agricultural cropping cycles derived from historical data and a global crop mask. Specifically, a vegetation health index (VHI) is defined as a weighted combination of deviations of NDVI and BT4 from the historical range of NDVI and BT4. Grid cells with a VHI value below 35% over a

growing season are considered as experiencing severe drought. The final ASI value is calculated as the percentage of crop or grassland pixels within each administrative unit affected by severe drought. Unlike the other hazard data used, these drought maps are not produced using extreme value modeling but calculated directly from the 39-year time series: a location recording at least one severe drought (as defined by the ASI) between 1984 and 2022 is considered exposed to a 39-year return period event.

For pluvial and fluvial floods, we use the Fathom Global 2.0 flood hazard maps<sup>16</sup>. The Fathom data depicts the maximum inundation depth of fluvial and pluvial floods at a resolution of 3 arcseconds for return periods ranging from 5 to 1,000 years. We use the undefended flood maps. While Fathom provides a defended option for fluvial flooding, it uses GDP as a proxy to set defense standards rather than the actual presence of flood defense structure. There is evidence that many low and middle-income countries do not have effective flood protection systems<sup>6,18,60</sup>. The Fathom data have global coverage between 56°S and 60°N. For coastal floods, we use hazard maps from Deltares since the Fathom data does not represent coastal flooding<sup>17</sup>. Coastal flooding is modelled using the same digital elevation model (MERIT DEM) at the same 3 arcsecond spatial resolution as Fathom 2.0, but forced by tide and storm surges (e.g., during a tropical cyclone). The Deltares dataset depicts the maximum depth of coastal flooding for return periods ranging from 0 to 250 years, with global coverage. A combined global flood hazard map was created for return periods ranging from 5 to 100 years by taking the maximum inundation depth of any flood type.

For heatwaves, we use modelled hazard maps from the World Bank Climate Change Knowledge Portal (CCKP) based on hourly ERA5 climate reanalysis data<sup>28</sup>. The probabilistic heatwave data depicts the 5-day average of the daily maximum Environmental Stress Index (ESI) at a resolution of 0.25 degrees for return periods ranging between 5 and 100 years. The ESI is an approximation for the Wet Bulb Globe Temperature (WBGT), derived from temperature, relative humidity and solar radiation<sup>61</sup>. The ESI formula was adjusted to correct for underestimation from solar radiation<sup>62</sup>.

For tropical cyclones, we use modelled hazard maps generated using the STORM (Synthetic Tropical cyclOne geneRation Model) synthetic resampling algorithm<sup>20,21</sup>. STORM is applied to 38 years of historical cyclone track data from the International Best Track Archive for Climate Stewardship (IBTrACS) to statistically extend the dataset to 10,000 years of cyclone activity. The dataset covers all tropical cyclone basins except the South Atlantic which has too few historical cyclone formations in this basin for adequate model fitting. The cyclone data depicts the maximum 10-minute average sustained wind speed at a resolution of 0.1 degrees for return periods ranging from 10 to 10,000 years.

### **Boundary data**

To aggregate gridded exposure data, we use boundary data corresponding with the smallest representative spatial units in household surveys used to derive vulnerability indicators. In many countries, these are admin-1 boundaries, but survey statistical regions are not necessarily aligned with administrative boundaries and vary between admin-2 and national

level. Subnational boundary data sources include Global Administrative Unit Layers (GAUL) 2015, Nomenclature of Territorial Units for Statistics (NUTS), GADM (v4.1), United Nations Common Operational Datasets, and National Statistical Offices (NSOs)<sup>63,64</sup>. The boundary data allows estimates aggregated from gridded spatial data to be merged with survey-based population vulnerability estimates.

## **Step 2 – Determining who is vulnerable**

The share of the population considered highly vulnerable is derived from both household surveys and spatial data. We identify those vulnerable based on these different types of data separately. The following sections detail the sources of data used to calculate survey-based vulnerability indicators and how they are fused together to calculate the share of the population vulnerable on any dimension (or combination of dimensions), typically at subnational level. The final section of this step describes the Rural Access Index spatial data and how it is used to estimate the population vulnerable in terms of access to services and markets.

### **Survey-based vulnerability data**

Six of the seven dimensions of vulnerability we consider are estimated using data from household surveys or similar population-based sources. For income, educational attainment, access to improved drinking water and access to electricity, we use household survey microdata from the World Bank’s Global Monitoring Database (GMD), a repository of multitopic income and expenditure household surveys used to monitor global poverty<sup>33</sup>.

The GMD’s harmonized microdata is used in the Poverty and Inequality Platform (PIP), the World Bank’s Multidimensional Poverty Measure (MPM), the Global Database of Shared Prosperity (GDSP). These poverty and inequality statistics are widely used in the economics and development literature. The household survey data are typically collected by national statistical offices in each country, and then compiled, processed, and harmonized to the extent possible such that levels and trends in poverty and other key sociodemographic attributes can be reasonably compared across and within countries over time<sup>34</sup>. All the data go through validity checks. Since we use the exact same surveys as those used to estimate official poverty statistics, the population considered *highly* vulnerable on the income dimension in our study corresponds precisely with the extreme poverty data published by the World Bank. Other dimensions correspond with published multidimensional poverty statistics. Much of the underlying microdata in GMD is not publicly available because surveys are owned by national governments or statistical offices and cannot be shared.

The income and consumption data are extrapolated or interpolated to a common reference year (e.g., 2021) following the method used by the World Bank’s Poverty and Inequality Platform (PIP) for global poverty monitoring<sup>65</sup>. The extrapolation uses growth rates from national accounts, either real GDP per capita or real Household Final Consumption Expenditure per capita and a passthrough rate of 0.7. This allows the share of the population

falling beneath a given poverty line to be calculated between and beyond the survey years which can be infrequent. For other indicators, we use survey data collected closest to the reference year as comparable lineup methods do not yet exist.

In a small number of countries where GMD surveys are missing variables on education, access to water or access to electricity, we use estimates from other data sources for subgroups of the population. These are fused into the GMD household surveys using the simulation method described in the next section. For primary education completion, we use UNESCO Institute for Statistics (UIS) estimates based on national population censuses and household and labor force surveys, which are reported at the urban/rural level<sup>66</sup>. For access to improved drinking water, we use estimates from WHO/UNICEF Joint Monitoring Programme (JMP), which are reported at rural/urban level and by subnational region and wealth quintile when available<sup>67</sup>. For access to electricity, we use the SDG indicator 7.1.1 estimates from the World Bank's Global Electrification Database (GED), reported at rural/urban level<sup>68</sup>. To improve country coverage, we assume universal access to improved water and electricity (i.e. no one is counted as highly vulnerable) if secondary data sources indicate more than 97% of the population have access.

For access to social protection, we use data from The Atlas for Social Protection (ASPIRE)<sup>32</sup>. The data includes the share of households that either receive social transfers or contribute to social insurance programs, since we want to capture those who will receive support in the event of a shock, even if they are not current beneficiaries. This indicator is based on household surveys when available, and administrative data or modelled estimates when survey data is incomplete. Estimates are reported for rural/urban and income quintile subgroups of the population, which we fuse into the GMD household surveys using the simulation method described in the next section. We assume no households are vulnerable on this dimension in high-income countries, which tend to have sophisticated social protection systems and are not included in ASPIRE.

For access to finance, we use individual level microdata from the Global Financial Inclusion Database (Findex)<sup>31</sup>. A household is considered vulnerable on this dimension if no household members have a bank or mobile money account. This indicator is estimated for rural/urban and income quintile subgroups of the population. Since Findex data is collected at individual level, we adjust estimates to household level to be consistent with other indicators. The adjustment is based on the number of adults in a household and a factor derived from examining countries where data on both household and individual ownership of accounts is available (see Supplementary Information). Household level estimates for each population subgroup are fused into GMD surveys using the simulation method described in the following section.

### **Fusing different sources of vulnerability data**

Estimating the share of households vulnerable on any dimension requires “fusing” data from different sources, since not all dimensions are available from the same GMD household survey. For instance, the social protection and financial inclusion dimensions are based on

ASPIRE and Findex, respectively. These indicators are available for population subgroups including rural/urban households, households in each welfare quintile and in some cases at subnational level. Based on these subgroup statistics, we use a simulation method to fuse indicators derived from other data sources into the household level GMD data. This allows us to estimate the share of the population vulnerable on any dimension (or a combination of multiple dimensions).

For each dimension not available in GMD, households are randomly assigned a vulnerability status (0/1) based on the share of households that are vulnerable in the population subgroup they belong to, estimated from other surveys,. This preserves summary statistics reported for each subset of the population, for example, the share of the poorest rural quintile without access to social protection in ASPIRE. The share of households vulnerable on any dimension (or a combination of dimensions) is then calculated at the level of the representative statistical unit. This random assignment and aggregation process is repeated 100 times to account for household heterogeneity within each subgroup. The average share of households vulnerable on any and each combination of dimensions is calculated across all simulations and used for the analysis.

### **Spatial vulnerability data**

For access to services and markets, we use gridded data produced to calculate the Rural Access Index (RAI) (SDG 9.1.1) for the Sustainable Development Report 2024<sup>69</sup>. RAI is defined as the proportion of the rural population living within 2km of an all-season road. The dataset is derived from road network maps (Open Street Map, Global Roads Inventory Project Database, and Microsoft BING – Road Detection Project) and other geospatial data such as slope and rainfall which is used to assess the all-season status of uncategorized roads<sup>70</sup>. The data indicates the share of the population in each grid cell more than 2 km from an all-season road. We calculate the population more than 2km from an all-season road at grid level by multiplying the RAI inaccessibility data (resampled to align with the population grid) with the population data. The resulting grid level estimate of the number of people vulnerable is aggregated to the statistical regions corresponding with surveys in the same way as exposure estimates.

### **Step 3 - Determining who is at risk**

To determine who is at risk, we combine exposure and vulnerability estimates from the previous steps (Extended Data Figure 5). This requires first aggregating the exposure data to the same population units represented by surveys.

The grid level exposure-urbanization estimates are aggregated spatially to the level of the survey statistical regions by overlaying boundary data, as described in step 1. The exposure estimates by degree of urbanization (7 categories) for each spatial unit are then aggregated to the rural/urban classification in the survey data by matching population shares. To estimate the rural population exposed, for example, we take the population weighted

exposure rate from the most rural degree of urbanization categories until we have accounted for the population share defined as rural according to the survey definition. Validation shows this method is effective at accounting for differences between rural/urban classifications (see Supplementary Information).

The spatially derived vulnerability data, measuring the population with low access to services and markets, is also classified by exposure status at grid level. This means we can directly estimate the population both exposed and vulnerable on this dimension, without making assumptions about the correlation between exposure and vulnerability within a larger geographic region. The grid level estimates are aggregated to the same population units as the survey-based vulnerability data in the same way as exposure, described above.

Once the exposure and vulnerability estimates represent the same spatial and rural/urban population units, the population at high risk in each unit (exposed to any hazard and vulnerable on any dimension) is calculated as:

$$high\_risk = risk_{RAI} + (exp - risk_{RAI}) \times vuln_{survey}$$

where  $risk_{RAI}$  is the population exposed and vulnerable on the low access dimension (based on spatial data),  $exp$  is the population exposed, and  $vuln_{survey}$  is the share of the population vulnerable on any survey-based dimension. This calculation assumes that survey-based vulnerability dimensions are not correlated with exposure within population units (nor with spatially defined vulnerability). Estimates are aggregated to country, region and global level by taking the population weighted sum across all survey units.

### **Sensitivity of results**

We check the sensitivity of results to several assumptions. The regional composition of the exposed population is similar when we use different intensity thresholds or return periods to define exposed locations (Extended Data Table 2 and Supplementary Information). The trend in the population at high risk is robust to restricting the sample to countries with data on all dimensions from within 3 years of both 2010 and 2021. We also estimate lower and upper bounds by assuming the minimum and maximum possible overlap between the exposed and vulnerable population, rather than assuming the vulnerable population are just as likely to be exposed as those not vulnerable within a spatial unit. Estimates of the global population at high-risk range from 16% to 23% for 2021 in these extreme lower and upper bound scenarios, compared to 19% in our preferred specification (see Supplementary Information).

### **Data Availability**

The datasets generated and/or analyzed during the current study are available at <https://doi.org/10.60572/9j17-9n52>. Source data are provided with this paper.

**Code Availability**

The code used to generate the analysis is available at <https://doi.org/10.60572/9j17-9n52>.

## References

1. Dang, H.A.H. and Dabalén, A.L. (2018). Is Poverty in Africa Mostly Chronic or Transient? Evidence from Synthetic Panel Data. *Journal of Development Studies* 55 (7): 1527–47.
2. Hallegatte, S., Bangalore, M., Bonzanigo, L., Fay, M., Kane, T., Narloch, U., Rozenberg, J., Treguer, D. & Vogt-Schilb, A. (2016). *Shock Waves: Managing the Impacts of Climate Change on Poverty*. Washington, DC: World Bank.
3. IPCC. (2023). *Climate Change 2023: Synthesis Report. Contribution of Working Groups I, II and III to the Sixth Assessment Report of the Intergovernmental Panel on Climate Change* [Core Writing Team, H. Lee and J. Romero (eds.)]. IPCC, Geneva, Switzerland, 184 pp., doi: 10.59327/IPCC/AR6-9789291691647.
4. Hallegatte, S., Vogt-Schilb, A., Rozenberg, J. et al. (2020). From Poverty to Disaster and Back: a Review of the Literature. *EconDisCliCha* 4, 223–247. <https://doi.org/10.1007/s41885-020-00060-5>
5. CDRI. (2023). *Global Infrastructure Resilience: Capturing the Resilience Dividend – A Biennial Report from the Coalition for Disaster Resilient Infrastructure*, New Delhi.
6. Hallegatte, S., Vogt-Schilb, A., Bangalore, M., & Rozenberg, J. (2017). *Unbreakable: Building the Resilience of the Poor in the Face of Natural Disasters*. Climate Change and Development. Washington, DC: World Bank. <http://hdl.handle.net/10986/25335>
7. Notre Dame Global Adaptation Initiative Country Index (ND-GAIN). (2024). University of Notre Dame.
8. Inter-Agency Standing Committee and the European Commission, INFORM REPORT 2024: 10 years of INFORM. (2024). Publications Office of the European Union, Luxembourg. <https://data.europa.eu/doi/10.2760/555548>, JRC136641.
9. Eckstein, D., Künzel, V. and Schäfer, L. (2021). *The global climate risk index 2021*. Bonn: Germanwatch.
10. Bündnis Entwicklung Hilft / IFHV (2024): *WordRiskReport 2024*. Berlin: Bündnis Entwicklung Hilft.
11. Doan, Miki Khanh (ORCID) Hill, Ruth (ORCID) Hallegatte, Stephane (ORCID) Corral Rodas, Paul Andres (ORCID) Brunckhorst, Ben James; Nguyen, Minh (ORCID) Freije-Rodriguez, Samuel (ORCID) Naikal, Esther G. (2023). *Counting People Exposed to, Vulnerable to, or at High Risk From Climate Shocks - A Methodology (English)*. Policy Research working paper 10619. Washington, D.C. : World Bank Group.
12. IPCC. (2022). *Climate Change 2022: Impacts, Adaptation, and Vulnerability. Contribution of Working Group II to the Sixth Assessment Report of the Intergovernmental Panel on Climate Change* [H.-O. Pörtner, D.C. Roberts, M. Tignor, E.S. Poloczanska, K. Mintenbeck, A. Alegría, M. Craig, S. Langsdorf, S. Lösschke, V. Möller, A. Okem, B. Rama (eds.)]. Cambridge University Press. Cambridge University Press, Cambridge, UK and New York, NY, USA, 3056 pp., doi:10.1017/9781009325844.
13. Van Hoolst, R., Eerens, H., Haesen, D., Royer, A., Bydekerke, L., Rojas, O., Li, Y. and Racionzer, P. (2016). FAO's AVHRR-based Agricultural Stress Index System (ASIS) for global drought monitoring. *International Journal of Remote Sensing*, 37(2), pp.418-439.
14. Kogan, F.N. (1995). Application of vegetation index and brightness temperature for drought detection. *Advances in space research*, 15(11), pp.91-100.
15. FAO. (2023). *Agricultural Stress Index System (ASIS): Historic Agricultural Drought Frequency (Global - 1Km)*. <http://www.fao.org/giews/earthobservation/>
16. Sampson, C., Smith, A. M., Bates, P. D., Neal, J. C., Alfieri, L., & Freer, J. E. (2015). A High-resolution Global Flood Hazard Model. *Water resources research*, 51(9), 7358-7381.
17. Deltares. (2021). *Planetary computer and Deltares global data: Flood Hazard Maps*. Deltares.
18. Rentschler, J., Salhab, M., & Jafino, B. A. (2022). Flood Exposure and Poverty in 188 Countries. *Nature Communications*, 13(1), 3527.
19. Huizinga, J., De Moel, H. and Szweczyk, W. (2017). *Global flood depth-damage functions: Methodology and the database with guidelines* (No. JRC105688). Joint Research Centre.
20. Bloemendaal, N., Haigh, I. D., de Moel, H., Muis, S., Haarsma, R. J., & Aerts, J. C. (2020). Generation of a Global Synthetic Tropical Cyclone Hazard Dataset Using STORM. *Scientific data*, 7(1), 40.
21. Bloemendaal, N., De Moel, H., Muis, S., Haigh, I. D., & Aerts, J. C. (2020). Estimation of Global Tropical Cyclone Wind Speed Probabilities Using the STORM Dataset. *Scientific data*, 7(1), 377.
22. Eberenz, S., Lüthi, S., & Bresch, D. N. (2021). Regional Tropical Cyclone Impact Functions for Globally Consistent Risk Assessments. *Natural Hazards and Earth System Sciences*, 21(1), 393-415.

23. Bloemendaal, N. and Koks, E.E. (2022). Current and Future Tropical Cyclone Wind Risk in the Small Island Developing States. In *Hurricane Risk in a Changing Climate* (pp. 121-142). Cham: Springer International Publishing.
24. International Organization for Standardization. (2017). *Ergonomics of the thermal environment— Assessment of heat stress using the WBGT (wet bulb globe temperature) index* (ISO Standard No. 7243:2017). <https://www.iso.org/standard/67188.html>
25. Foster, J., Smallcombe, J. W., Hodder, S., Jay, O., Flouris, A. D., Nybo, L., & Havenith, G. (2021). An advanced empirical model for quantifying the impact of heat and climate change on human physical work capacity. *International Journal of Biometeorology*, 65, 1215-1229. <https://doi.org/10.1007/s00484-021-02105-0>
26. Kjellstrom, T., Freyberg, C., Lemke, B., Otto, M., & Briggs, D. (2018). Estimating population heat exposure and impacts on working people in conjunction with climate change. *International Journal of Biometeorology*, 62(3), 291-306.
27. Cheng, Y., Lung, S., & Hwang, J.-S. (2019). New approach to identifying proper thresholds for a heat warning system using health risk increments. *Environmental Research*, 170, 282-292.
28. World Bank, Climate Change Knowledge Portal (2024). Environmental Stress Index. <https://climateknowledgeportal.worldbank.org/>.
29. Hersbach, H., Bell, B., Berrisford, P., Hirahara, S., Horányi, A., Muñoz-Sabater, J., Nicolas, J., Peubey, C., Radu, R., Schepers, D. and Simmons, A., (2020). The ERA5 global reanalysis. *Quarterly Journal of the Royal Meteorological Society*, 146(730), pp.1999-2049.
30. Dijkstra, L., Florkczyk, A.J., Freire, S., Kemper, T., Melchiorri, M., Pesaresi, M. and Schiavina, M., (2021). Applying the degree of urbanisation to the globe: A new harmonised definition reveals a different picture of global urbanisation. *Journal of Urban Economics*, 125, p.103312.
31. Demirgüç-Kunt, Asli, Leora Klapper, Dorothe Singer, Saniya Ansar. (2022). *The Global Findex Database 2021: Financial Inclusion, Digital Payments, and Resilience in the Age of COVID-19*. Washington, DC: World Bank.
32. World Bank. (2024). ASPIRE (Atlas of Social Protection: Indicators of Resilience and Equity). July 2024 update.
33. World Bank. (2024). Poverty and Inequality Platform (version 20240627\_2017\_01\_02\_PROD). Available at <https://pip.worldbank.org>.
34. World Bank. (2024). Poverty and Inequality Platform Methodology Handbook. Edition 2024-09. Available at <https://datanalytics.worldbank.org/PIP-Methodology/>.
35. Hallegatte, S., J. Rentschler, and J. Rozenberg. (2019). *Lifelines: The resilient infrastructure opportunity*. Washington, DC: World Bank.
36. Burgess, Robin, and Dave Donaldson. (2010). "Can Openness Mitigate the Effects of Weather Shocks? Evidence from India's Famine Era." *American Economic Review*, 100 (2): 449–53.
37. Dobermann, T. (2023). How building up the human capital of the world's poor can help lessen the climate crisis. *LSE Business Review*.
38. Hoffmann, R., & Muttarak, R. (2017). Learn from the Past, Prepare for the Future: Impacts of Education and Experience on Disaster Preparedness in the Philippines and Thailand. *World Development*, 96, 32-51.
39. Muttarak, R., & Lutz, W. (2014). Is Education a Key to Reducing Vulnerability to Natural Disasters and hence Unavoidable Climate Change? *Ecology and Society*, 19(1). <https://www.jstor.org/stable/26269470>
40. Muttarak, R., & Pothisiri, W. (2013). The role of education on disaster preparedness: case study of 2012 Indian Ocean earthquakes on Thailand's Andaman Coast. *Ecology and Society* 18(4): 51. <http://dx.doi.org/10.5751/ES-06101-180451>
41. Jack, W., & Suri, T. (2014). Risk Sharing and Transactions Costs: Evidence from Kenya's Mobile Money Revolution. *American Economic Review*, 104 (1): 183-223.
42. Batista, C., & Vicente, P. C. (2023). Is mobile money changing rural Africa? Evidence from a field experiment. *Review of Economics and Statistics*, 1-29.
43. Riley, E. (2018). Mobile money and risk sharing against village shocks. *Journal of Development Economics*, 135, 43-58. <https://doi.org/10.1016/j.jdeveco.2018.06.015>

44. De Janvry, A., Finan, F., Sadoulet, E., & Vakis, R. (2006). Can conditional cash transfer programs serve as safety nets in keeping children at school and from working when exposed to shocks? *Journal of Development Economics*, 79(2), 349-373. <https://doi.org/10.1016/j.jdeveco.2006.01.013>
45. Abay, K. A., Yonzan, N., Kurdi, S., & Tafere, K. (2023). Revisiting Poverty Trends and the Role of Social Protection Systems in Africa during the COVID-19 Pandemic. *Journal of African Economies*, 32(Supplement\_2), ii44-ii68. <https://doi.org/10.1093/jae/ejac041>
46. Gehrke, E. (2019). An Employment Guarantee as Risk Insurance? Assessing the Effects of the NREGS on Agricultural Production Decisions. *The World Bank Economic Review*, World Bank Group, vol. 33(2), pages 413-435.
47. Banerjee, A., Faye, M., Krueger, A., Niehaus, P., & Suri, T. (2020). Effects of a Universal Basic Income during the Pandemic. Working paper, University of California San Diego.
48. Ivaschenko, O., Doyle, J., Kim, J., Sibley, J., & Majoka, Z. (2020). Does ‘Manna from Heaven’ Help? The Role of Cash Transfers in Disaster Recovery—Lessons from Fiji after Tropical Cyclone Winston. *Disasters* 44 (3): 455–76.
49. Pople, A., Hill, R., Dercon, S., & Brunckhorst, B. (2021). Anticipatory Cash Transfers in Climate Disaster Response. Working Paper 6, Centre for Disaster Protection, London.
50. Londoño-Velez, J., & Querubin, P. (2022). The Impact of Emergency Cash Assistance in a Pandemic: Experimental Evidence from Colombia. *The Review of Economics and Statistics*, MIT Press, vol. 104(1), pages 157-165, March.
51. World Bank. (2022c). *Poverty and Shared Prosperity 2022: Correcting Course*. Washington, D.C.: The World Bank.
52. Gentilini et al. (2022). *Social Protection and Jobs Responses to COVID-19: A Real-Time Review of Country Measures*. World Bank.
53. Beazley, R., Marzi, M., & Steller, R. (2021). Drivers of Timely and Large-Scale Cash Responses to COVID19: what does the data say? *Social Protection Approaches to COVID-19 Expert Advice Service (SPACE)*, DAI Global UK Ltd, United Kingdom.
54. Rentschler, J., Avner, P., Marconcini, M., Su, R., Strano, E., Vousdoukas, M., & Hallegatte, S. (2023). Global evidence of rapid urban growth in flood zones since 1985. *Nature*, 622(7981), 87-92.
55. Schiavina, M., Freire, S., Alessandra C., & MacManus, K. (2023). GHS-POP R20–3A - GHS Population Grid Multitemporal (1975-2030). European Commission, Joint Research Centre (JRC) [Dataset] <https://doi.org/10.2905/2FF682-5B5B-4A22-8F40-C41DA8332CFE>
56. Freire, S., MacManus, K., Pesaresi, M., Doxsey-Whitfield, E. and Mills, J., (2016). Development of new open and free multi-temporal global population grids at 250 m resolution. *Population*, 250, p.33.
57. Chen, R., Yan, H., Liu, F., Du, W., & Yang, Y. (2020). Multiple global population datasets: Differences and spatial distribution characteristics. *ISPRS International Journal of Geo-Information*, 9(11), 637. <https://doi.org/10.3390/ijgi9110637>
58. Schiavina, M., Melchiorri, M., & Pesaresi, M. (2023). GHS-SMOD R20–3A - GHS Settlement Layers, Application of the Degree of Urbanisation Methodology (stage I) to GHS-POP R2023A and GHSBUILT-S R2023A, multitemporal (1975-2030). European Commission, Joint Research Centre (JRC) [Dataset] <https://doi.org/10.2905/A0DF7A6F-49DE-46EA-9BDE-563437A6E2BA>
59. World Bank, World Development Indicators. (2024). “Population, total”. [Dataset]. <http://data.worldbank.org/indicator/SP.POP.TOTL>
60. Rozenberg, J., & Fay, M. (2019). *Beyond the Gap: How Countries Can Afford the Infrastructure They Need while Protecting the Planet*. Sustainable Infrastructure. Washington, D.C.: The World Bank.
61. Moran, D. S., Pandolf, K. B., Shapiro, Y., Heled, Y., Shani, Y., Mathew, W. T., & Gonzalez, R. R. (2001). An environmental stress index (ESI) as a substitute for the wet bulb globe temperature (WBGT). *Journal of thermal biology*, 26(4-5), 427-431.
62. Kong, Q., & Huber, M. (2022). Explicit calculations of wet-bulb globe temperature compared with approximations and why it matters for labor productivity. *Earth's Future*, 10(3), e2021EF002334.
63. Food and Agricultural Organization of the United Nations. (2015). *Global Administrative Unit Layers (GAUL)*. <http://www.fao.org/geonetwork>.
64. University of California, Berkeley. (2022). *Global Administrative Areas Version 4.1*. [www.gadm.org](http://www.gadm.org).

65. Mahler, Daniel Gerszon, R Andrés Castañeda Aguilar, and David Newhouse. (2022). “Nowcasting Global Poverty.” *The World Bank Economic Review* 36 (4): 835-56. <https://doi.org/10.1093/wber/lhac017>.
66. UNESCO Institute for Statistics (UIS). (2024). [Dataset]. <https://uis.unesco.org/bdds>. Accessed: April 2024.
67. United Nations Children’s Fund (UNICEF) and World Health Organization (WHO). (2024). Joint Monitoring Programme for Water Supply, Sanitation and Hygiene (JMP). <https://washdata.org/data>.
68. IEA, IRENA, UNSD, World Bank, WHO. (2023). Tracking SDG 7: The Energy Progress Report. World Bank, Washington DC.
69. Sachs, J. D., G. Lafortune, and G. Fuller. (2024). “The SDGs and the UN Summit of the Future. Sustainable Development Report 2024.” <https://doi.org/10.25546/108572>.
70. Iablonovski, G., Drumm, E., Fuller, G. and Lafortune, G. (2024). A global implementation of the rural access index. *Frontiers in Remote Sensing*, 5, p.1375476.

## **Acknowledgements**

We are thankful for comments from an internal World Bank advisory group chaired by Luis Felipe Lopez-Calva and Jennifer Sara to develop the methodology. We are grateful for inputs from the CCKP and ASPIRE teams at the World Bank, and from the UN Sustainable Development Solutions Network. The findings, interpretations and conclusions expressed in this paper are entirely ours. These findings do not necessarily represent the views of the World Bank and its affiliated organizations, or those of the Executive Directors of the World Bank or the governments they represent.

## **Author information**

### *Authors and Affiliations*

#### **The World Bank, Washington, DC, USA**

Ruth Hill, Nisan Gorgulu, Ben Brunckhorst, Minh Cong Nguyen, Stephane Hallegatte & Esther Naikal.

### *Contributions*

The authors randomized the author ordering (R.H., N.G., B.B., M.C.N., S.H., E.N.). All authors contributed to the paper.

### *Corresponding authors*

Correspondence to Ben Brunckhorst ([bbrunckhorst@worldbank.org](mailto:bbrunckhorst@worldbank.org)).

## **Ethics declarations**

### *Competing interests*

The authors declare no competing interests.

**Additional information**

Supplementary Information is available for this paper.

## Extended data figures and tables

**Extended Data Table 1: Population exposed to four hazards, by region (2021)**

Region	Total population (millions)	Share of population exposed (%)						
		Cyclone	Drought	Flood	Heatwave	Any	2+	3+
East Asia & Pacific	2370	17.1	13.7	13.7	53.6	<b>69.1</b>	25.9	3.0
Europe & Central Asia	924	0.2	21.5	6.6	0.4	<b>27.1</b>	1.5	0.0
Latin America & Caribbean	655	8.0	14.8	6.4	9.9	<b>33.9</b>	4.7	0.4
Middle East & North Africa	486	0.0	9.0	9.8	19.5	<b>34.5</b>	3.6	0.2
North America	370	7.2	16.9	3.9	8.8	<b>31.1</b>	5.3	0.4
South Asia	1902	6.5	17.1	12.4	82.1	<b>87.0</b>	28.6	2.4
Sub-Saharan Africa	1181	0.4	27.0	4.2	11.6	<b>38.2</b>	4.9	0.3
<b>World</b>	<b>7889</b>	<b>7.8</b>	<b>17.4</b>	<b>9.8</b>	<b>40.1</b>	<b>57.0</b>	<b>16.4</b>	<b>1.6</b>

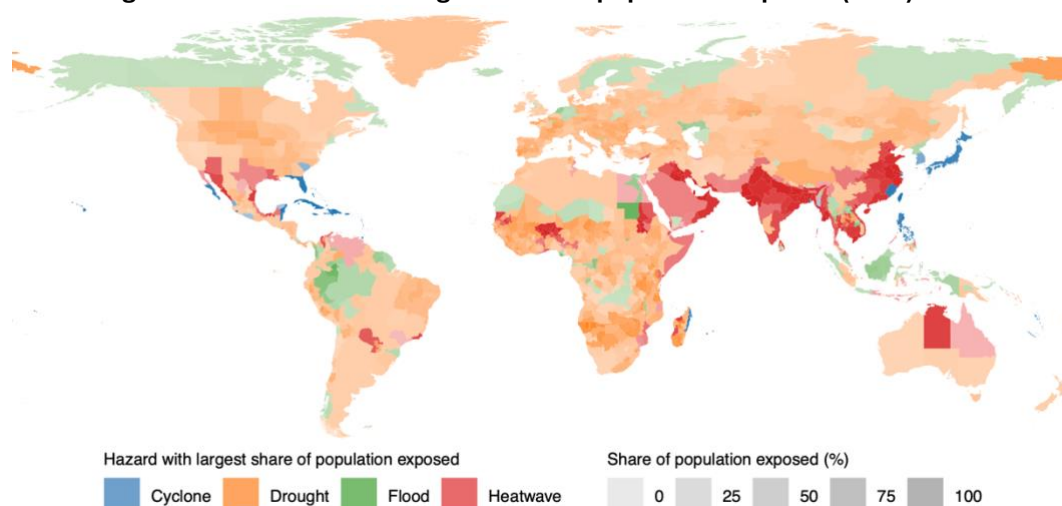
Notes: Exposure is defined using thresholds in Table 1.

**Extended Data Table 2: Population exposed to four hazards, by region (2021,  $\geq 5\%$  annual frequency)**

Region	Total population (millions)	Share of population exposed (%)						
		Cyclone	Drought	Flood	Heatwave	Any	2+	3+
East Asia & Pacific	2370	3.6	9.8	6.6	45.4	<b>55.5</b>	9.6	0.4
Europe & Central Asia	924	0.1	15.3	3.4	0.2	<b>18.6</b>	0.5	0.0
Latin America & Caribbean	655	0.3	10.6	3.2	7.0	<b>19.8</b>	1.2	0.0
Middle East & North Africa	486	0.0	8.8	3.9	17.6	<b>28.2</b>	1.9	0.1
North America	370	0.0	13.0	3.2	2.8	<b>18.3</b>	0.7	0.0
South Asia	1902	0.0	15.5	5.2	77.9	<b>83.0</b>	15.1	0.5
Sub-Saharan Africa	1181	0.0	22.6	2.1	4.9	<b>27.7</b>	1.8	0.0
<b>World</b>	<b>7889</b>	<b>1.1</b>	<b>13.9</b>	<b>4.6</b>	<b>34.9</b>	<b>47.2</b>	<b>7.1</b>	<b>0.3</b>

Notes: Exposure is defined using intensity thresholds in Table 1, but an annual frequency of at least 5%.

**Extended Data Figure 1: Hazard with the largest share of population exposed (2021)**



Notes: Lighter shades represent a lower share of the population exposed to that hazard.

**Extended Data Table 3: Population exposed to four hazards by degree or urbanization (2021)**

Degree of urbanization	Total Population (millions)	Share of population exposed (%)							
		Cyclone	Drought	Flood	Heatwave	Any	2+	3+	
Rural	Very low density rural	465	3.6	70.1	8.2	24.2	<b>77.5</b>	25.2	3.3
	Low density rural	975	4.5	75.5	8.3	31.7	<b>82.8</b>	32.1	5.0
	Rural cluster	414	3.3	74.9	8.1	27.4	<b>81.8</b>	28.6	3.3
Urban cluster	Suburban or peri-urban	1445	7.4	0.0	11.9	53.3	<b>58.5</b>	13.4	0.7
	Semi-dense urban cluster	226	4.3	0.0	8.1	28.4	<b>35.3</b>	5.2	0.3
	Dense urban cluster	907	6.2	0.0	11.2	37.9	<b>45.2</b>	9.6	0.6
Urban centre	Urban centre	3460	10.6	0.0	9.5	42.0	<b>48.0</b>	13.2	0.9

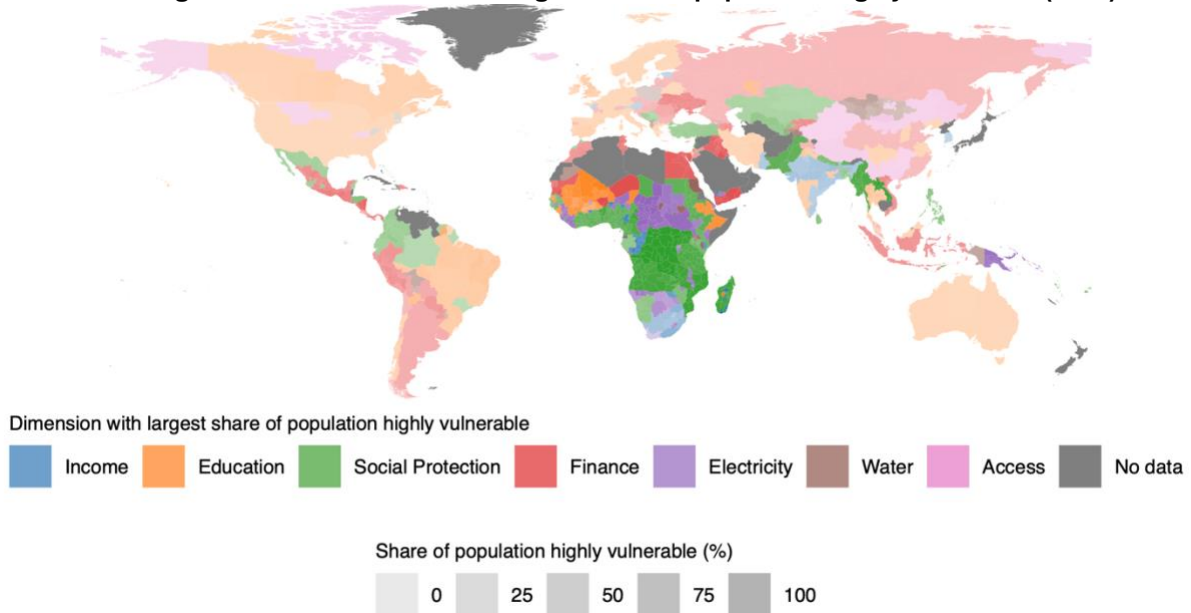
Notes: Exposure is defined using thresholds in Table 1.

**Extended Data Table 4: Population highly vulnerable on seven dimensions, by region (circa 2021)**

Region	Total Population (millions)	Share of population highly vulnerable (%)									
		Income	Education	Finance	Social protection	Electricity	Water	Access	Any	2+	3+
East Asia & Pacific	2182	1.0	2.7	7.6	6.5	1.0	1.7	1.1	<b>17.0</b>	3.3	0.9
Europe & Central Asia	917	0.4	2.0	5.9	7.0	0.0	0.7	0.2	<b>14.7</b>	1.3	0.1
Latin America & Caribbean	608	4.5	8.5	17.0	17.6	2.4	1.8	0.5	<b>40.0</b>	9.3	2.1
Middle East & North Africa	356	5.6	9.1	38.4	14.4	3.2	3.4	0.7	<b>51.5</b>	15.3	5.2
North America	370	0.0	0.9	0.0	0.0	0.0	0.0	0.0	<b>0.9</b>	0.0	0.0
South Asia	1862	11.4	8.6	13.1	13.8	1.5	1.0	0.3	<b>36.1</b>	10.1	2.6
Sub-Saharan Africa	1159	37.6	33.3	29.6	71.0	45.3	31.1	7.9	<b>90.5</b>	69.1	48.4
<b>World</b>	<b>7454</b>	<b>9.7</b>	<b>9.5</b>	<b>14.0</b>	<b>19.4</b>	<b>8.0</b>	<b>6.0</b>	<b>1.7</b>	<b>35.7</b>	<b>15.9</b>	<b>8.9</b>

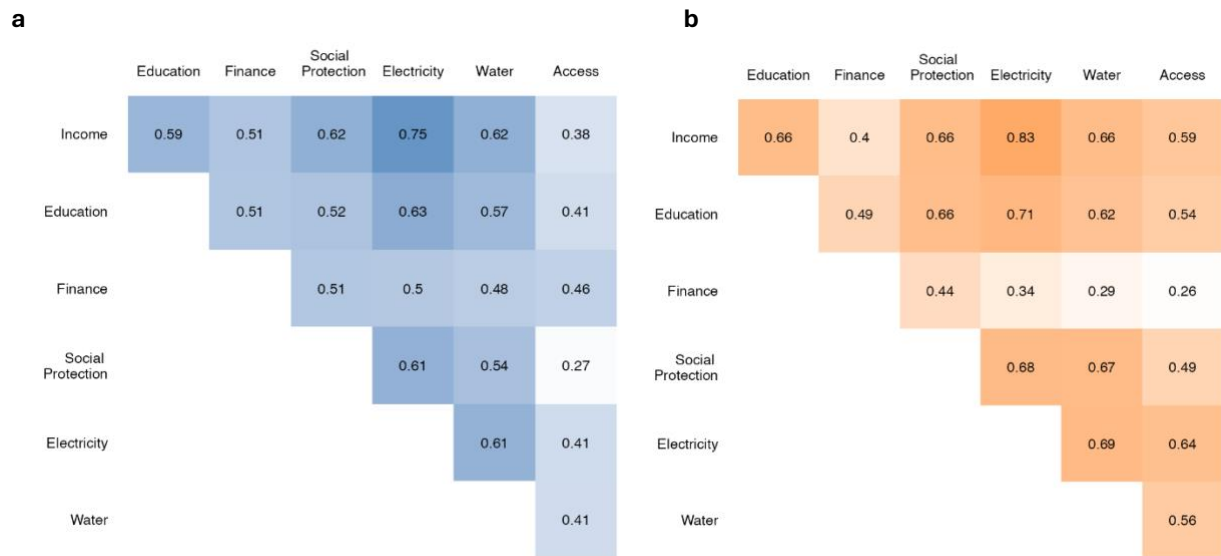
Notes: The sample includes 160 countries with vulnerability data available.

**Extended Data Figure 2: Dimension with the largest share of population highly vulnerable (2021)**



Notes: Lighter shades represent a lower share of the population highly vulnerable on that dimension.

**Extended Data Figure 3: Correlation between vulnerability dimensions (2021)**



**a.** Correlation in share of population highly vulnerable across dimensions at subnational level (N = 3,481). **b.** Correlation in share of population highly vulnerable across dimensions at national level (N = 160).

**Extended Data Table 5: Population exposed to any hazard and highly vulnerable, by region**

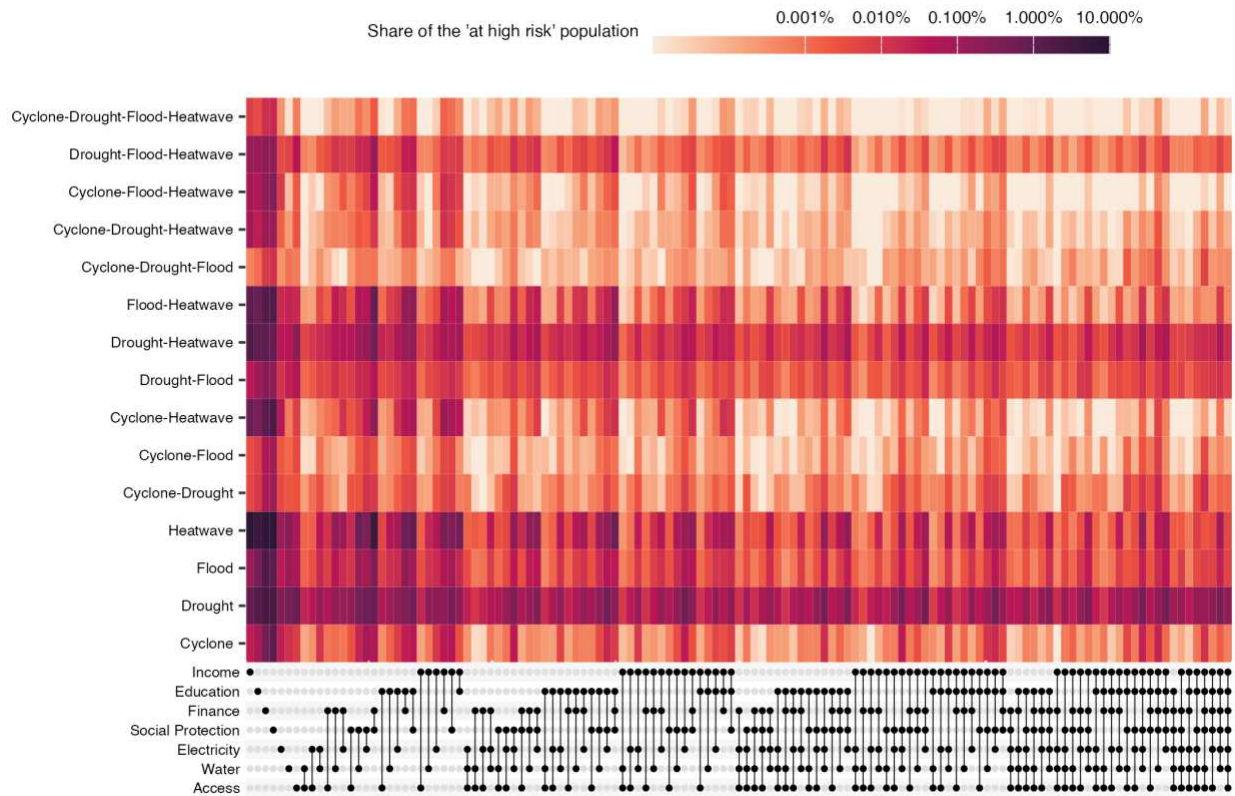
2021												
Region	Total Population (millions)	Share of population exposed and highly vulnerable (%)										
		Income	Education	Finance	Social protection	Electricity	Water	Access	Any	2+	3+	
East Asia & Pacific	2182	0.5	1.7	4.2	4.6	0.6	0.8	0.8	<b>10.6</b>	1.8	0.5	
Europe & Central Asia	917	0.1	0.5	1.6	1.8	0.0	0.2	0.1	<b>4.0</b>	0.4	0.0	
Latin America & Caribbean	608	2.2	3.7	6.3	7.1	1.7	1.2	0.3	<b>15.6</b>	4.7	1.4	
Middle East & North Africa	356	1.6	3.9	15.2	4.5	0.9	1.8	0.2	<b>19.7</b>	5.8	1.7	
North America	370	0.0	0.2	0.0	0.0	0.0	0.0	0.0	<b>0.2</b>	0.0	0.0	
South Asia	1862	10.5	7.4	11.6	12.0	1.2	0.6	0.2	<b>31.9</b>	8.8	2.1	
Sub-Saharan Africa	1159	16.1	16.2	13.0	26.9	19.9	14.0	5.9	<b>36.1</b>	29.7	22.1	
<b>World</b>	<b>7453</b>	<b>5.5</b>	<b>5.4</b>	<b>7.6</b>	<b>9.5</b>	<b>3.7</b>	<b>2.8</b>	<b>1.2</b>	<b>19.4</b>	<b>8.1</b>	<b>4.3</b>	

2010												
Region	Total Population (millions)	Share of population exposed and highly vulnerable (%)										
		Income	Education	Finance	Social protection	Electricity	Water	Access	Any	2+	3+	
East Asia & Pacific	2153	7.2	11.4	15.0	4.0	1.6	6.6	0.8	<b>32.1</b>	10.5	3.1	
Europe & Central Asia	883	0.3	3.1	6.4	1.8	0.1	0.4	0.1	<b>9.0</b>	3.0	0.3	
Latin America & Caribbean	538	3.0	6.0	15.6	7.1	2.3	3.0	0.3	<b>23.6</b>	8.8	3.2	
Middle East & North Africa	287	0.8	4.8	19.2	4.6	0.9	2.0	0.2	<b>24.2</b>	6.2	1.4	
North America	343	0.3	0.1	0.0	0.0	0.0	0.0	0.0	<b>0.4</b>	0.0	0.0	
South Asia	1632	23.6	18.1	39.2	11.8	21.2	8.0	0.2	<b>66.3</b>	36.2	14.9	
Sub-Saharan Africa	864	18.8	17.4	25.0	28.0	29.9	15.8	5.9	<b>39.4</b>	35.4	29.4	
<b>World</b>	<b>6700</b>	<b>10.8</b>	<b>11.4</b>	<b>20.5</b>	<b>8.8</b>	<b>9.8</b>	<b>6.5</b>	<b>1.1</b>	<b>35.7</b>	<b>18.1</b>	<b>8.8</b>	

Notes: The sample includes 160 countries with vulnerability data available. Exposure is defined using thresholds in Table 1.

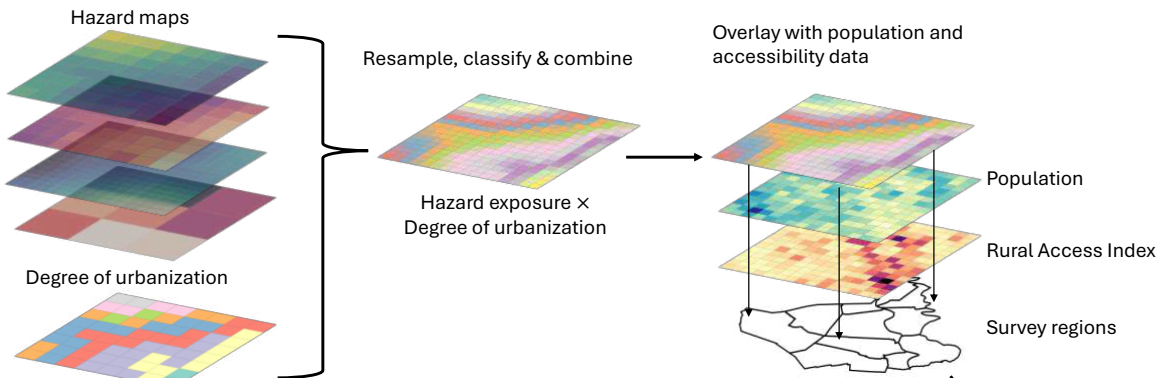
**Extended Data Figure 4: Population exposed and highly vulnerable by hazard and dimension combination**



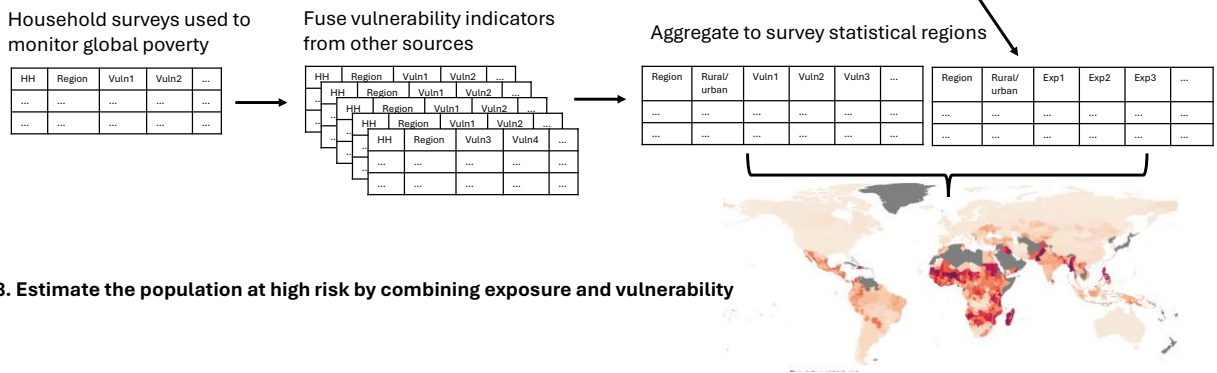
*Notes:* The heatmap illustrates the relative share of the population at high risk exposed to each combination of hazards and highly vulnerable on each combination of dimensions using thresholds defined in the study. Each row corresponds to a specific combination of the four hazard types. The columns represent different combinations of dimensions of vulnerability. The color intensity depicts the share of the population using a logarithmic scale for contrast, darker colors indicate more of the population having a specific hazard exposure and combination of vulnerabilities.

## Extended Data Figure 5: Summary of method

### 1. Identify the population exposed using spatial data



### 2. Identify the population that is highly vulnerable using household surveys



### 3. Estimate the population at high risk by combining exposure and vulnerability

## Supplementary Files

This is a list of supplementary files associated with this preprint. Click to download.

- [03SupplementaryInformationR1.docx](#)